Biomaterials 156 (2018) 107–120

Contents lists available at ScienceDirect

Biomaterials

journal homepage: www.elsevier.com/locate/biomaterials

Mechanistic insights into the role of glycosaminoglycans in delivery of polymeric nucleic acid nanoparticles by molecular dynamics simulations

Deniz Meneksedag-Erol [a, c], Tian Tang [a, b, **], Hasan Uludağ [a, c, d, *]

[a] Department of Biomedical Engineering, University of Alberta, Edmonton, AB, Canada
[b] Department of Mechanical Engineering, University of Alberta, Edmonton, AB, Canada
[c] Department of Chemical and Materials Engineering, University of Alberta, Edmonton, AB, Canada
[d] Faculty of Pharmacy and Pharmaceutical Sciences, University of Alberta, Edmonton, AB, Canada

ARTICLE INFO

Article history:
Received 23 June 2017
Received in revised form
2 November 2017
Accepted 21 November 2017
Available online 22 November 2017

Keywords:
siRNA
Polyethylenimine
Polymeric nanoparticle
Heparin
Glycosaminoglycan
Polynucleotide delivery
Molecular dynamics

ABSTRACT

Delivery of polynucleotide-based therapeutics into target cells involves interactions with glycosaminoglycan chains that are located on cell membrane milieu. Mechanisms governing glycosaminoglycan-mediated changes in the nanoparticulate structures of polymer-polynucleotide complexes are unknown, and cannot be fully elucidated without atomistic level details of molecular interactions. We selected a representative nanoparticulate system consisting of a short interfering RNA (siRNA)-polyethylenimine complex, and performed all-atom molecular dynamics simulations with the prototypical glycosaminoglycan heparin. We monitored the binding between the complex constituents and the heparin, and identified key features contributing to the response of the siRNA nanoparticles to heparin. We observed three main metastable states that the siRNA nanoparticles might visit in the presence of heparin, which can be translated into different functional outcomes. By correlating our data with the widely different and seemingly contradictory roles previously assigned to glycosaminoglycans, this study provides unique insights into the discrepancies in the experimental literature concerning the role of glycosaminoglycans in the polymeric nanoparticle delivery.

1. Introduction

Gene therapy with polynucleotide-based therapeutic agents holds considerable promise in a range of genetic and acquired diseases, including cancer. For functional delivery, polynucleotides are formulated into nanoparticulate structures by drug carriers for the protection of the polynucleotide cargo while facilitating its translocation through the plasma membrane. Owing to their safety and versatility, synthetic cationic polymers are the most utilized carriers. For a therapeutic benefit, either locally or systemically administered polynucleotides must be internalized by the targeted cells, remain intact in endocytic compartments, and disassemble from the polymeric carriers to be transported to the appropriate sub-cellular compartment. Extracellular matrix components and cell membrane molecules have been recognized to be involved in the process of polynucleotide delivery, as the cellular uptake of the polynucleotide nanoparticles is influenced by their interaction with the membrane milieu. Glycosaminoglycans (GAGs) located on the cell surface and in extracellular matrix, are a class of structurally heterogeneous complex polysaccharides (10–100 kDa [1]), having a high anionic charge density due to the presence of carboxyl and sulfate groups [2]. The most common GAGs are heparin/heparan sulfate (HS), chondroitin/dermatan sulfate (CS/DS), keratan sulfate (KS), and hyaluronic acid (HA) [2–4].

The role of the GAGs on the uptake of polynucleotide nanoparticles has been controversial and long debated. Previous studies have reported widely different and seemingly contradictory conclusions on the involvement of GAGs in the polynucleotide delivery pathway. On one hand, sulfated GAGs have been attributed beneficial effects in the delivery of polynucleotide nanoparticles. It was suggested that GAGs can act as “receptors”, upon the observation of

* Corresponding author. Department of Chemical and Materials Engineering, University of Alberta, Edmonton, AB, Canada.
** Corresponding author. Department of Mechanical Engineering, University of Alberta, Edmonton, AB, Canada.
E-mail addresses: meneksed@ualberta.ca (D. Meneksedag-Erol), tian.tang@ualberta.ca (T. Tang), hasan.uludag@ualberta.ca (H. Uludağ).

https://doi.org/10.1016/j.biomaterials.2017.11.037
0142-9612/

a significant reduction in the transfection efficiency of nanoparticles *in vitro* [5] and *in vivo* [6] after the alteration of cell surface GAGs by either treatment with chlorate that decreases the sulfation of GAGs [7], or by enzymatic removal of the GAGs with GAG lyases. Moreover, chlorate treated cells was shown to display increased levels of cationic lipid associated cytotoxicity while addition of exogenous sulfated GAGs to the medium could reverse this toxic effect, suggesting that GAGs can reduce the cytotoxicity of the nanoparticles by shielding their high cationic charge [8]. On the other hand, exogenous GAGs were reported to decrease *in vitro* transfection efficiency of the polynucleotide nanoparticles [5,6,9]. The delivery agents that are the most susceptible to the deleterious effects of GAGs were identified as the polycationic carriers with buffering capability, such as polyamidoamine (PAMAM) dendrimers, polyethylenimine (PEI), and dioctadecylamidoglycylspermine (DOGS); while fusogenic lipids such as 1,2-dioleyl-3-phosphatidylethanolamine (DOPE) were observed to resist better the GAG associated inhibitory events [9]. The inhibitory effects of the GAGs were attributed to their capability to alter or disrupt the integrity of nanoparticulate complexes. Many physicochemical studies carried out in this context [9–12] have reported partial relaxation of the nanoparticles or complete release of the polynucleotide cargo depending on GAG concentration and the physical properties of the GAG. In addition, binding of free GAGs to the nanoparticles was suggested to sequester the cationic charge of the nanoparticles, preventing them from establishing electrostatic interactions with the cell membrane or “GAG receptors” on the cell surface, hence blocking the cellular entry [6]. GAGs could also affect intracellular trafficking/dissociation of the polynucleotide nanoparticles. Confocal microscopy studies have shown that exogenous GAGs could be internalized by the cells in complex with the carriers [13] and polynucleotide nanoparticles [14], and the complex-bound GAGs may direct the nanoparticles into unfavorable endosomes for functional translation [15,16]. Accordingly, these reported dual roles of GAGs on polymeric polynucleotide delivery systems creates a discrepancy in our understanding of their exact role.

The molecular details of the interactions between the GAGs and polynucleotide nanoparticles are obscure. The factors governing the extent of their interaction and the subsequent effects of these interactions on the functional performance are not well defined. The lack of a mechanistic understanding on the conditions leading the change in biological performance hinders the development of functional polynucleotide delivery systems that could make use of the beneficial aspects of the GAGs, while withstanding their inhibitory effects. Molecular dynamics (MD) simulations can provide atomic resolution information on the dynamic evolution of the biological systems, which could not be readily attainable with most experimental tools. In this study, we performed a series of all-atom MD simulations on model polynucleotide nanoparticle − GAG systems. We used a short interfering RNA (siRNA) as a representative polynucleotide and PEI as a prototypical polymeric carrier, while heparin served as a prototypical GAG. The simulation systems were designed based on the experimental literature with the aim of creating a series of scenarios that the siRNA/PEI/heparin ternary systems might exist. At the all-atom level, Barnard and coworkers developed an approach to estimate a carrier's ability to release a gene cargo by comparing the carrier's binding affinity to DNA and to heparin sulfate from individual one-on-one binding simulations [17], without directly addressing question of complex disassembly. While this approach is useful to make comparative analysis among different carriers, without running the complex three partite simulations it does not provide any mechanistic details on complex disassembly and the behavior of the polymeric polynucleotide nanoparticles in the presence of heparin. To the best of our knowledge, our study is the first attempt to simulate the interactions of heparin with polynucleotide nanoparticles using all-atom MD simulations. We aim to shed light on the ambiguity in the experimental literature through detailed analysis of heparin interactions with the nanoscale siRNA-PEI complexes and heparin-mediated changes on the conformational states of the complexes, and correlating them with the current experimental data.

2. Methods

2.1. Simulated systems

The specific siRNA simulated is designed for P-glycoprotein mRNA silencing [18]: sense: 5′-CAGAAAGCUUAGUACCAAATT-3′; antisense: 5′-UUUGGUACUAAGCUUUCUGTC-3′. It carries a total charge of −40 in the fully deprotonated state. The initial structure of the siRNA is adopted from our previous study [19]. We studied two PEIs differing in molecular weight (MW): 568 Da and 1874 Da (Fig. 1a and b). 568 Da PEI consists of 13 amine groups, of which 6 are protonated; 1874 Da PEI has 43 amine groups and 20 of them are protonated (indicated in Fig. 1a and b). The exact protonation state of PEI under physiological conditions is unknown; previous experimental works have determined varying protonation ratios, ranging from 10 to 20% [20,21] to ~50% [22,23]. Ziebarth and Wang's “computational titration” through Monte Carlo simulations [24] has shown that linear PEI has a protonation ratio of 55% under physiological conditions. From isothermal titration calorimetry (ITC) assays, Utsuno and Uludağ reported the fraction of protonated PEI Ns to be 47% at pH = 6, and 33% at pH = 7 [25]. Considering that in the context of cancer therapy the target of the siRNA based therapeutics is malignant tumors, the conditions of the tumor environment should also be taken into account. The extracellular pH of human tumors is known to be slightly on the acidic side [26–28]; the pH values reported in the literature range from 5.85 to 7.68 [29]. From these considerations, in this study, we chose PEI protonation ratio to be 46% corresponding to the protonation state at pH = 6[25], consistent with our previous studies [19,30–34]. The initial structures of the PEIs are adopted from our previous studies [30,32], where the pre-equilibration of the structures were performed for 6 ns for the 568 Da PEI [30], and 50 ns for the 1874 Da PEI [32] with MD package of NAMD [35]. We investigated two heparin molecules differing in length: a dodecasaccharide (12-mer), and a henicosasaccharide (21-mer). The structures of heparin (Fig. 1c and d) consist of alternating units of N,O6-disulfo-glucosamine (GlcNS(6S)) and 2-O-sulfo-alpha-L-idopyranuronic acid (IdoA2S) residues. The charge of the heparin molecule is dependent on its length; the 12-mer heparin carries a total charge of −24, whereas the 21-mer heparin molecule carries a total charge of −42. The initial coordinates of the 12-mer heparin molecule are adopted from the NMR solution structure of heparin under the PDB code: 1HPN, Model 1[36], and the two ends of the molecule were saturated with hydrogen (H). The initial structure of the 21-mer heparin molecule was built upon adopting the atomic coordinates from the same PDB code and extending the length of the heparin chain by increasing the number of repeating IdoA2S − GlcNS(6S) disaccharides using Schrödinger's Maestro software [37]. Both the 12-mer and 21-mer heparin molecules were equilibrated for 10 ns (restrained) + 10 ns (free) with MD package of NAMD [35] (Section 1; Supporting Information). The structures of the heparin molecules at the end of the simulations were adopted as input structures to the main simulations with the siRNA complexes.

We investigated two groups of siRNA–PEI complexes with different polymer/siRNA charge ratios: one group with polymer/siRNA charge ratio ≥ 1, and the other with polymer/siRNA charge ratio <1. Changing the polymer/siRNA charge ratio (Table 1) was

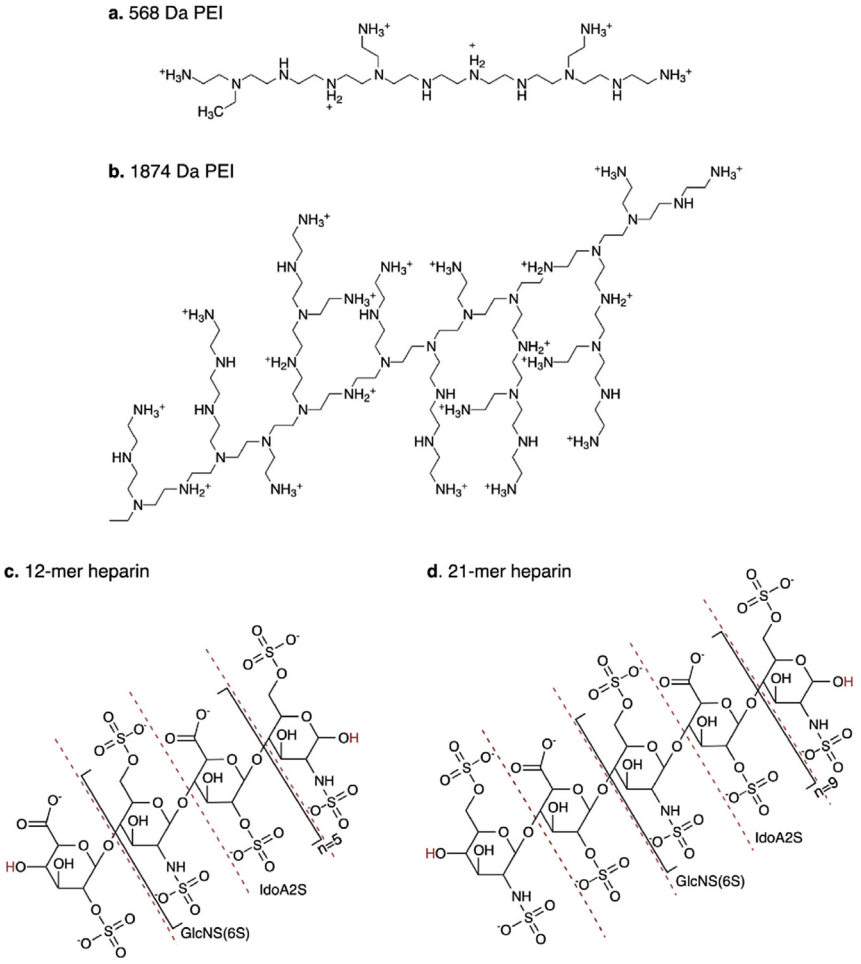

Fig. 1. Chemical structures of the simulated molecules, (**a**) 568 Da PEI, (**b**) 1874 Da PEI, (**c**) 12-mer heparin, and (**d**) 21-mer heparin. Protonation sites of the PEIs are indicated with (+) in (**a**) and (**b**). The saturation sites in the heparin molecules are highlighted in red, and the number of the repeating IdoA2S – GlcNS(6S) disaccharide is denoted with n in (**c**) and (**d**). (For interpretation of the references to colour in this figure legend, the reader is referred to the web version of this article).

Table 1
Information on the siRNA – PEI – heparin ternary systems simulated in this study.

System	PEI MW (Da)	PEI/siRNA charge ratio	Heparin length	Number of heparins	Simulation box volume (nm^3)	Heparin concentration (mM)	Heparin/PEI charge ratio
C1-7sh	568	1.05	12-mer	7	1129.5	10.3	2.0
C2-2sh	568	0.15	12-mer	2	793.8	4.2	4.0
C2-5sh	568	0.15	12-mer	5	762.3	10.9	10.0
C2-2lh	568	0.15	21-mer	2	981.2	3.4	7.0
C3-7sh	1874	1.00	12-mer	7	1761.0	6.6	2.1
C4-5sh	1874	0.50	12-mer	5	968.2	8.6	3.0
C4-2lh	1874	0.50	21-mer	2	876.4	3.8	2.1

achieved by changing the MW of the PEI and/or the number of PEI molecules in the complexes. Complex 1 (C1) consisted of 2 siRNA and 14 PEI (568 Da) molecules. In the initial configuration of C1 (Fig. 2a, left and middle panels), 2 siRNA molecules were placed at a center of mass (COM) distance of 17.7 Å. Two PEIs were then placed amidst the 2 siRNAs, and the remaining 12 PEIs were placed symmetrically to surround the siRNAs. Upon solvation with TIP3P water and adding a proper amount of K^+ and Cl^- ions to achieve 150 mM salt concentration, the system was simulated for 10 ns (restrained) + 50 ns (free) for the complexation to occur. From the final configuration of C1 at the end of the simulation (Fig. 2a, right panel), the initial structure of the system Complex 2 (C2) was generated (Fig. 2b, left and middle panels). This was done by removing the 12 PEI molecules in the periphery of the C1's final structure, along with all the water molecules and ions, while keeping the 2 PEI molecules bridging the 2 siRNAs. Upon re-solvation and re-ionization (150 mM KCl), C2 was simulated for 10 ns (restrained) + 10 ns (free). Complex 3 (C3) consists of 2 siRNA and 4 PEI (1874 Da) molecules. In the initial configuration of C3 (Fig. 2c, left and middle panels), 2 siRNA molecules were placed at COM distance of 17.7 Å. Two PEIs were then positioned amidst the 2 siRNAs, and the remaining 2 PEIs were placed symmetrically to the periphery of the siRNAs. The system was solvated, ionized with 150 mM KCl and simulated for 10 ns (restrained) + 50 ns (free). The final configuration of C3 is given in Fig. 2c, right panel. By removing the 2 peripheral PEIs along with all the water molecules and ions and keeping the 2 PEIs bridging the two siRNAs, the initial structure of Complex 4 (C4) was built (Fig. 2d, left and middle panels). System

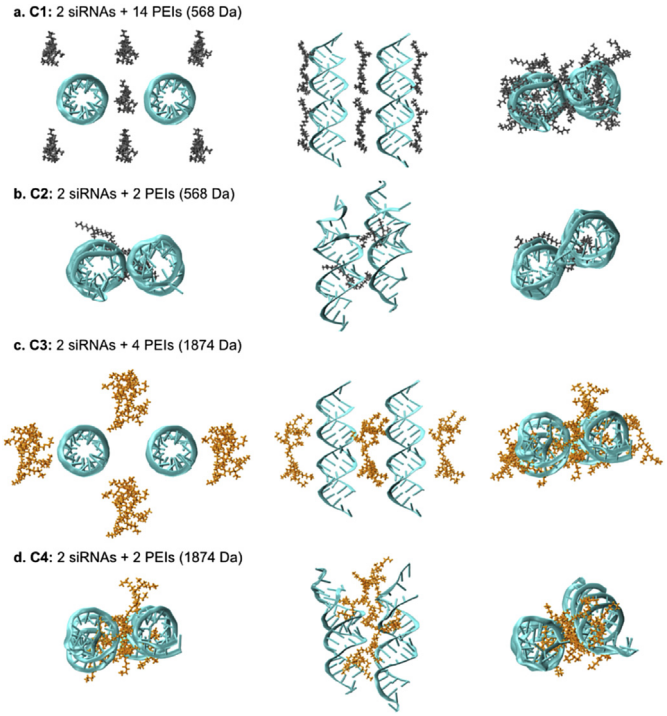

Fig. 2. Initial (left: top view; and middle: side view) and final (right: top view) configurations of the simulated complexes; (**a**) C1, (**b**) C2, (**c**) C3, and (**d**) C4. siRNAs are given in cyan, 568 Da PEIs are in gray, and 1874 Da PEIs are in orange. Water and ions are removed for clarity. (For interpretation of the references to colour in this figure legend, the reader is referred to the web version of this article.)

C4 was re-solvated and re-ionized, and then simulated for 10 ns (restrained) + 10 ns (free). The final configurations of systems C1, C2, C3 and C4 (right panel of Fig. 2a–d, respectively) were then adopted as input structures to further simulations with heparins.

To explore heparin's effects on the complexes, seven simulation systems were designed to contain different numbers of heparin molecules (Table 1). All the siRNA-PEI-heparin ternary systems possess a net negative charge; the charge ratio of the heparin to PEI molecules in each system is given in the last column of Table 1. To design the initial structures of the siRNA-PEI-heparin ternary systems (Fig. 3a, c–f, h, i; left panel), a desired number of heparin molecules was added to the pre-formed siRNA-PEI complexes, corresponding to the final configurations of systems C1, C2, C3 and C4. To facilitate the discussion herein, the simulation systems are labeled to include the complex identifier, the number of heparins, and the length of the heparin molecule, respectively. For this purpose, 12-mer heparin is represented with lower case letters "sh (short heparin)" and 21-mer heparin with lower case letters "lh (long heparin)", both appended to the number of heparins in the system name. To explore the influence of the MW of the PEIs, the simulated systems are divided into two main groups that contain PEIs of 568 Da and 1874 Da. The first group consists of systems bearing the 568 Da PEI: C1-7sh, C2-2sh, C2-5sh and C2-2lh; and the second group has the 1874 Da PEI as the carrier: C3-7sh, C4-5sh, C4-2lh. Within the first group, C2-2sh and C2-5sh differ only by the number of heparin molecules, which allows us to investigate the influence of heparin amount on the proposed roles of heparin. Systems C2-2sh and C2-2lh differ only by the length of the heparin molecule, which allows the exploration of possible consequences of heparin chain length (or MW) variation on the properties/dynamics of the complexes. To systematically explore the effect of the PEI MW, comparisons will be made in three pairs of systems: C1-7sh vs. C3-7sh, C2-5sh vs. C4-5sh, and C2-2lh vs. C4-2lh, as the two systems in each pair consist of the same number of heparins of the same chain length. All the heparin containing systems were simulated for 10 ns (restrained) + 250 ns (free), upon solvation in a rectangular box of TIP3P water with a margin of 15 Å from all sides, and ionization with 150 mM KCl.

Two additional simulations were performed in the absence of heparins to serve as a "control". Specifically, from the final structure of the C2 (Fig. 2b, right panel), the starting structure of Complex 2 control (C2 ctl) was constructed by removing all the water molecules and ions (Fig. 3b, left panel). Upon re-solvation and re-ionization (150 mM KCl), system C2 ctl was simulated for 10 ns (restrained) + 250 ns (free). Complex 4 control (C4 ctl, Fig. 3g, left panel) is constructed from C4, and simulated in a similar way. These systems will be compared to their heparin bearing counterparts; i.e., system C2 ctl serves as a control to C2-2sh, C2-5sh and C2-2lh, and system C4 ctl is the control to C4-5sh and C4-2lh.

2.2. Simulation details

The force field for the PEI molecules was adopted from a CHARMM format force field which was generated and validated with *ab initio* calculations in our previous works [30,32,38]. The force field for the heparin molecule was devised by following the CHARMM General Force Field (CGENFF) methodology [39]. The procedure we followed for the development and validation of heparin's force field is given in detail in Section 1 and 2 of Supporting Information, respectively. Briefly, the topology of the main building blocks of heparin was generated by analogy to the selected parent and model compounds in CHARMM36 additive all-atom carbohydrate force field [40]. Extended CHARMM36 general force field (CGENFF36) of sulfonyl-containing compounds [41] was used for the sulfamate group ($NHSO_3^-$) in GlcNS(6S). The default topology of the sulfamate group was modified to include the adjusted partial atomic charges retrieved from quantum mechanical calculations at HF/6-31G(d) level using Gaussian 09 [42]. Bond, angle, torsion, and van der Waals parameters were adopted from the existing parameters of the selected analogous compounds in CHARMM36 additive all-atom carbohydrate force field [40] and CGENFF36[41]; and the assignment of the missing parameters was done by following the CGENFF methodology [39]. CHARMM27 force field [43–46] was used for all the other molecules.

All simulations were performed with MD package of NAMD [35]. A time step of 2 fs, periodic boundary conditions (PBC), particle mesh Ewald (PME) [47] for full electrostatics, a cut-off of 12 Å for van der Waals and pairwise interactions, and SHAKE algorithm [48] to constrain the bonds involving H atoms were used in all simulations. All systems were first minimized for 5000 steps, and then gradually heated from 0 K to 300 K within 20 ps, with a harmonic restraint of 10 kcal/mol·Å^2 on non-H atoms of the solute. Systems were further simulated for 10 ns while keeping the restraint on solute's non-H atoms. The restraint was then removed, and NPT simulations were performed for 50 ns for complexes C1 and C3, 10 ns for complexes C2 and C4, and 250 ns for all the siRNA-PEI-heparin ternary systems as well as their controls. Temperature control was achieved with Langevin dynamics thermostat with thermostat damping coefficient of 10 ps^{-1} for all the non-H atoms. Nose–Hoover–Langevin barostat with damping time scale of 100 fs and Langevin piston oscillation period of 200 fs was used for pressure control. VMD [49] was used for the visualization and analysis of the simulation trajectories.

3. Results and discussion

The final configurations of the siRNA-PEI-heparin ternary systems as well as their controls are shown in the right panel of Fig. 3.

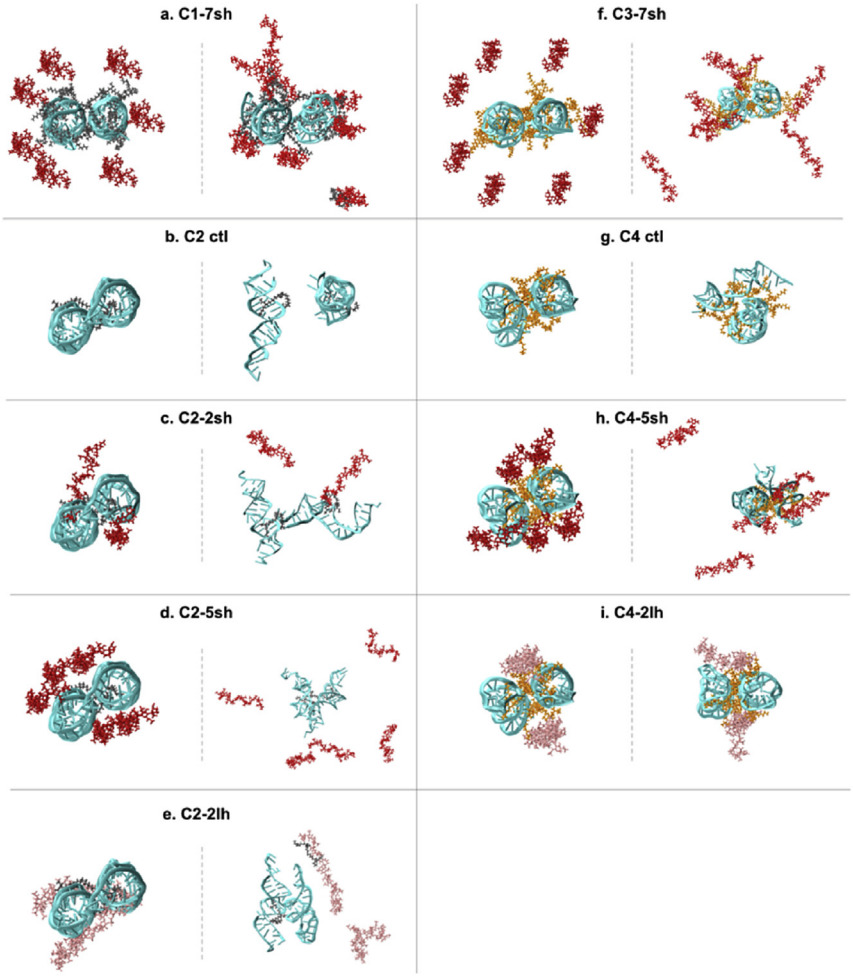

Fig. 3. The initial (left) and final (right) configurations of the simulated siRNA-PEI-heparin ternary systems and their controls (**a**) C1-7sh, (**b**) C2 ctl, (**c**) C2-2sh, (**d**) C2-5sh, (**e**) C2-2lh, (**f**) C3-7sh, (**g**) C4 ctl, (**h**) C4-5sh, and (**i**) C4-2lh. The color coding of the molecules is as follows: cyan, siRNA; gray, 568 Da PEI; orange, 1874 Da PEI; red, 12-mer heparin; pink, 21-mer heparin. Water and ions are removed for clarity. (For interpretation of the references to colour in this figure legend, the reader is referred to the web version of this article).

The conformational states of the ternary systems were vastly varied depending on: (*i*) the physical properties of siRNA-PEI complexes, namely PEI/siRNA charge ratio and PEI MW, and (*ii*) heparin properties, namely the length of the heparin chain and the number of heparin molecules. We investigated the effect of heparin on the dynamics of the complexes, as well as the atomistic details of the interactions formed between the PEI and heparin to elucidate the mechanism of heparin mediated changes on the siRNA complexes.

3.1. Dynamics of siRNA complexes in the presence of heparin

3.1.1. siRNA dynamics

The integrity of the siRNA complexes en-route to cells is a critical parameter affecting the desired therapeutic outcome. If the complex integrity is disrupted through disintegration of the protective carrier vectors, and the siRNAs get exposed to surrounding environment, the delivery performance can get adversely affected either through the degradation of the exposed siRNAs by the nucleases, or poor cellular uptake due to high anionic charge of the siRNAs. To assess the compactness of the complexes in the absence and presence of heparin molecules, we first monitored the time course of the center of mass (COM) distance between the two siRNAs. Under practical conditions, gel electrophoresis mobility shift assays are commonly used to monitor the stability of the siRNA complexes against the exogenous GAGs, where a fully dissociated complex would result in a band whose intensity is equal to that of the free siRNA sample. In a fully dissociated complex, it is expected that the siRNAs are no longer in an aggregated form, and are separated from each other. Here, COM distance between the two siRNAs was chosen as the parameter to quantify the compactness of the complexes, where a significant increase in the COM distance would signal the complete disassembly of the complex.

In Fig. 4a, we plotted the COM distance as a function of the simulation time, along with the average COM distance over the last 50 ns of the simulations in Fig. 4b. It can be seen from Fig. 4a that five out of seven simulated systems display COM distances that are fluctuating from 25 Å to 35 Å throughout the simulations; whereas two systems, C2 ctl and C2-2sh, exhibited COM separation beyond 35 Å. The latter two systems share the same complex composition (C2) comprising a low MW PEI, and possess a PEI/siRNA charge ratio below unity. For quantification purposes, we defined the time for siRNA separation when the COM distance between the two siRNA molecules reaches 35 Å and shows an overall increasing trend beyond this value. Following this definition, the control system C2 ctl was observed to experience siRNA separation with a sudden jump in the COM distance above 40 Å at around 100 ns, after which an increasing trend with fluctuations was observed reaching to

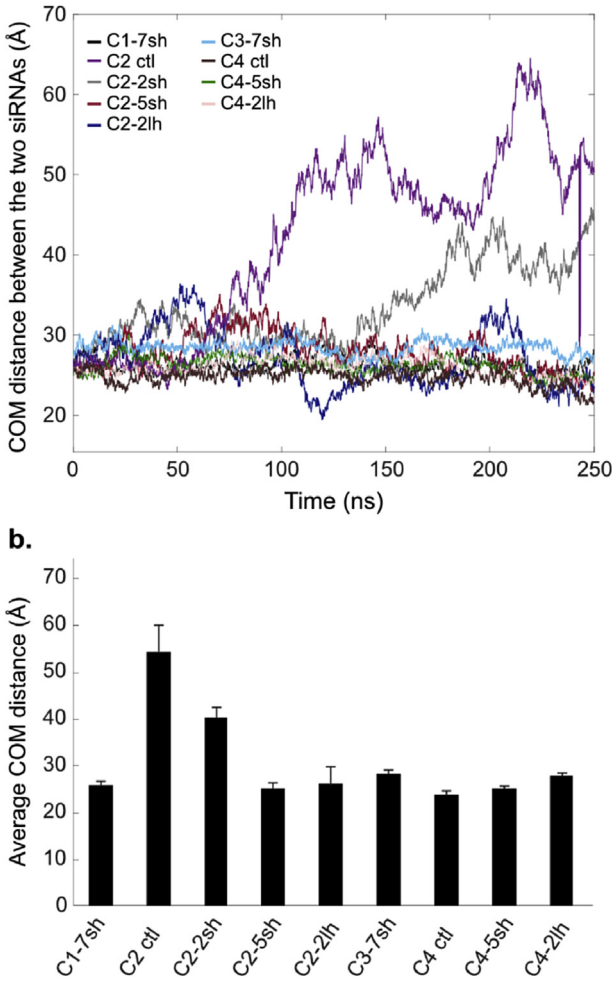

Fig. 4. **(a)** Time evolution, and **(b)** average values over the final 50 ns of the simulations of the COM distance between the two siRNA molecules.

54.37 ± 5.45 Å on average over the last 50 ns. On this regard, with time-resolved fluorescence spectroscopy techniques, Vuorimaa and coworkers [50] have previously shown that DNA possesses different states when in complex with PEI. They proposed a 2-step mechanism for PEI-DNA binding where DNA first undergoes an intermediate state between free and loosely bound states at low PEI/DNA charge ratios, and transitions to fully bound state when PEI/DNA charge ratio is higher. Their findings might serve as the experimental validation for the COM separation seen in C2 ctl, given that the PEI/siRNA charge ratio is 0.15 in this system.

In comparison to C2 ctl, system C2-2sh experienced less separation (with an average value of 40.05 ± 2.38 Å for the last 50 ns) starting at ~170 ns. Increasing the number of heparin molecules from low to moderate (C2-5sh), or the length of the heparin molecule from 12-mer to 21-mer (C2-2lh) prevented the separation of the siRNAs. Compared with C2 ctl (no heparin), the presence of heparin molecules did not expedite (C2-2sh), or cause (C2-5sh, C2-2lh) siRNA separation; however, these observations could be attributed to MD-related limitations such as finite simulation box size and the use of PBC. PBC are used to introduce the bulk properties of the solution, where the primitive simulation cell is replicated in all directions to create infinite images of the simulation box [51]. As our simulations consist of disordered many-body systems, use of PBC may bring in an “artificial periodicity” [52]. Our simulation boxes are quite spacious (15 Å water layer from all edges of the box), but the presence of free heparin molecules close to the edges increases their chances of interaction with their own images. This interaction might impose a repulsive force on the primitive cell, confining the contents of the simulation box to a limited space and hindering the necessary particle motions needed for siRNA separation in C2-5sh.

Among the low MW PEI systems, increasing the PEI/siRNA charge ratio above unity (C1-7sh) increased the stability of complexes, so that no separation was evident. High MW (1874 Da) PEI systems, namely C3-7sh, C4 ctl, C4-5sh, and C4-2lh, did not elicit siRNA separation, and displayed fairly stable COM separation through the simulations.

Visual examination of our simulation trajectories revealed an interesting mechanism involving the torsional motion of the siRNAs, i.e., change in relative orientation of the principal axes of the two siRNAs, accompanying siRNA separation. The torsional motion may impose a negative impact on the complex stability arising from (*i*) the weakening of the polyion bridging among multiple siRNAs, and (*ii*) the generation of an accessible area between the siRNAs for binding of heparin molecules to exposed PEIs. Thus, the relative orientation of the siRNAs was monitored based on the cosine of the angle θ (cos θ) between the two siRNA molecules. To do so, we defined a vector in each siRNA molecule by connecting two atoms at the opposite ends of the siRNA's two strands (C1′ of the 18th residue in each strand). We then measured the angle θ between the two vectors as a function of the simulation time. $\theta = 0^\circ$ ($\cos\theta = 1$) represents the configuration of two parallel siRNA molecules, whereas $\theta = 90^\circ$ ($\cos\theta = 0$) corresponds to the two siRNAs being perpendicular to each other. Fig. 5 shows the time evolution of $\cos\theta$ in the simulated systems. All systems consist of two siRNA molecules which are initially aligned parallel ($\cos\theta = 1$). We defined the transition from parallel to perpendicular orientation when $\cos\theta$ is reduced to 0.7, and shows an overall decreasing trend beyond. Such a transition indicates the complexes being “partially relaxed”. Partial relaxation was seen in systems C2 ctl, C2-2sh, C2-5sh, and C4 ctl. Among these four systems, separation of the siRNAs took place at ~100 ns and ~170 ns in C2 ctl and C2-2sh, respectively. The time of transition from parallel to perpendicular siRNA orientation is at ~140 ns in both systems, revealing that the torsional motion of the siRNAs could either accompany or follow the siRNA separation, or could be a preceding mechanism to complex disassembly via the partial relaxation of the complex. System C2-5sh displayed a very early transition (at ~50 ns) in siRNA torsional motion in comparison with others, although siRNA separation was not present within the simulated time frame. The onset of partial relaxation was detected at ~230 ns in system C4 ctl, which comprises 1874 Da PEI as the carrier and PEI/siRNA charge ratio below unity. Compared with C2 ctl (both systems are in the absence of heparin), increasing the PEI MW from 568 Da to 1874 Da increased the overall stability of the complex. However, complex relaxation is still seen to some extent in this system given that PEI/siRNA charge ratio is below unity.

Among the remaining systems, C3-7sh displayed the least amount of torsion, followed by C4-2lh and C4-5sh, all consisting of 1874 Da PEI. The systems with 568 Da PEI, C1-7sh and C2-2lh, did not display the signs of partial relaxation, although the periods of high fluctuation in C2-2lh should be noted. These observations thereby highlighted the two distinct influences on the siRNA torsional motion. First, the course of relaxation was highly dependent on PEI MW as well as PEI/siRNA charge ratio. Second, increasing the heparin length in the 568 Da PEI systems impeded the partial relaxation of the complexes (C2-2sh vs. C2-2lh).

3.1.2. PEI dynamics

To investigate the PEI dynamics accompanying separation or partial relaxation of the siRNAs, we examined polyion bridging in

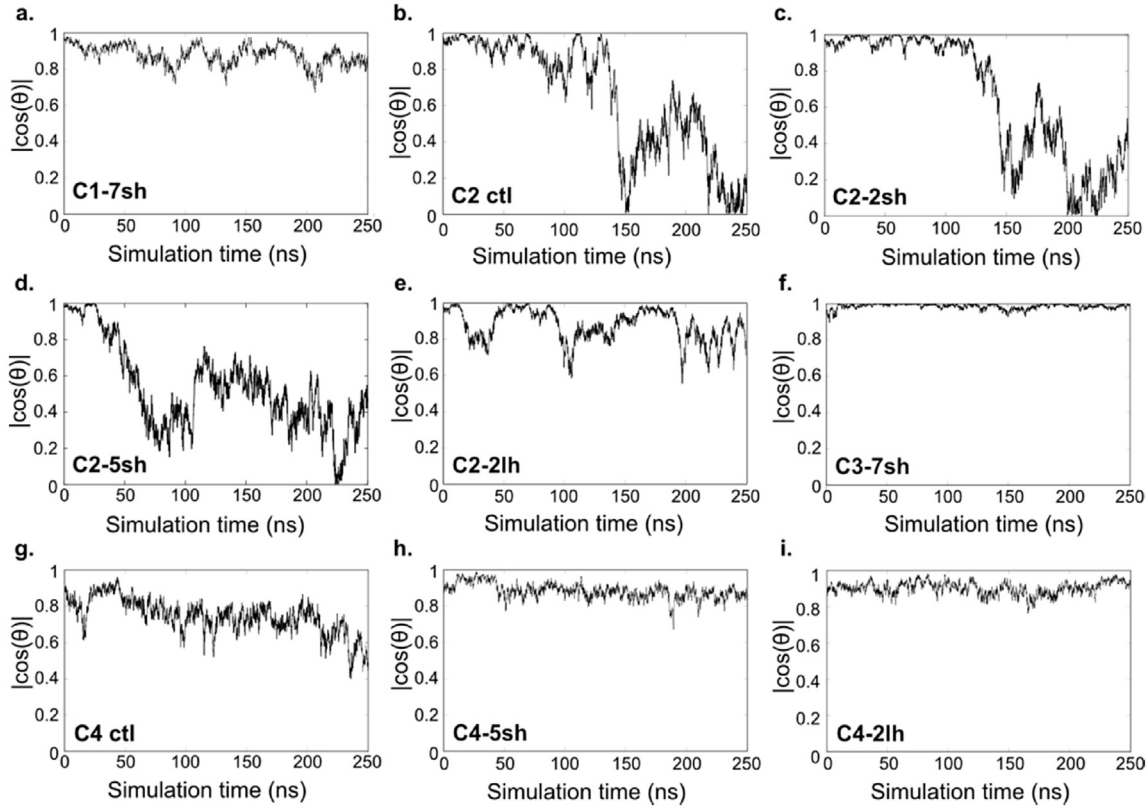

Fig. 5. Absolute value of cos θ between the two siRNA molecules as a function of the simulation time in (**a**) C1-7sh, (**b**) C2 ctl, (**c**) C2-2sh, (**d**) C2-5sh, (**e**) C2-2lh, (**f**) C3-7sh, (**g**) C4 ctl, (**h**) C4-5sh, and (**i**) C4-2lh.

C2 ctl, C2-2sh, C2-5sh, and C4 ctl, where the complexes displayed signs of instability. The polyion bridging pattern in the remaining systems can be found in Figs. S6 and S7 (Supporting Information). Fig. 6 shows the number of PEI N atoms within 4 Å of any N/O atoms of siRNA or heparin, as a function of the simulation time. Here, 4 Å represents the distance in which a direct H-bond between PEI amines and siRNA and/or heparin N/O could be formed [33]. Each subfigure contains two plots corresponding to the two PEIs in each system (labeled as PEI-1 and PEI-2 respectively). In these systems, we intentionally kept the two PEI molecules amidst the two siRNAs to serve as a bridge while constructing the initial configurations. Each plot has a different number of curves representing the two siRNA, and two or more of the heparin molecules (each heparin is labeled with a number, for example, heparin-1). To quantify polyion bridging, the following definitions have been made: (*i*) a PEI is defined as bound to an siRNA (or heparin) if it has at least one N atom within 4 Å of any of the N/O of the siRNA (or heparin); (*ii*) a polyion bridge forms when one PEI molecule is bound to two siRNA molecules simultaneously.

In system C2 ctl (Fig. 6a), PEI-1 and PEI-2 were found to bridge the two siRNA molecules up until 76 ns and 87 ns, respectively. Subsequently, each PEI maintained their interactions with their closest siRNA, losing their interaction with the other siRNA. As discussed above, C2 ctl showed siRNA COM separation at around 100 ns, followed by torsional motion of the siRNAs starting at ~140 ns. The loss of polyion bridging thus preceded both siRNA COM separation and the torsional motion, and may indicate the reason for siRNA separation. The presence of two heparin molecules in system C2-2sh (Fig. 6b) slightly extended the bridging brought by the PEI-1 (from 76 ns to 110 ns). PEI-1 was bound to heparin-1 since the beginning of the simulation, and this interaction was further strengthened upon the loss of PEI-1's contact with siRNA-1. PEI-1 maintained its bound state to siRNA-2 and heparin-1 past 110 ns. As observed in system C2 ctl, the decrease in polyion bridging preceded both the COM separation of the siRNAs as well as siRNA torsional motion, which took place at ~170 ns and 140 ns, respectively. Presence of heparin did not break the polyion bridge formed by PEI-2. However, the strength of this bridge was substantially weakened, fluctuating around 1 or 2 bound Ns (out of 13 N atoms in total) to siRNA-2 past 166 ns. Increasing the number of heparin molecules, on the other hand (C2-5sh, Fig. 6c), did not lead to the loss of the bridges formed by the PEIs, except in PEI-2 during the early stages of the simulation. The bridging performance of PEI-2 is again significantly weakened, in fact non-existent between 40 and 100 ns, and fluctuating around 1 or 2 N atoms bound to siRNA-2 past 100 ns. In addition, neither of the PEIs are bound to any heparin molecule in system C2-5sh despite the higher number of heparin molecules than that of C2-2sh. Although showing the onset of partial relaxation towards the end of the simulation, system C4 ctl (Fig. 6d) displayed a strong and consistent polyion bridging throughout the simulation. This system contains 1874 Da PEI which forms stronger contacts with the siRNAs, regardless of the PEI/siRNA charge ratio being below unity.

3.2. Interactions of PEI with heparin and siRNAs

The siRNA and heparin are both anionic in nature, capable of forming electrostatic interactions with the cationic PEI. The physicochemical characteristics of each molecule, however, are distinctly different from each other. The type of the anionic group (phosphate groups of siRNA vs. sulfate and carboxylate groups of heparin), the spacing between the charged groups, as well as the

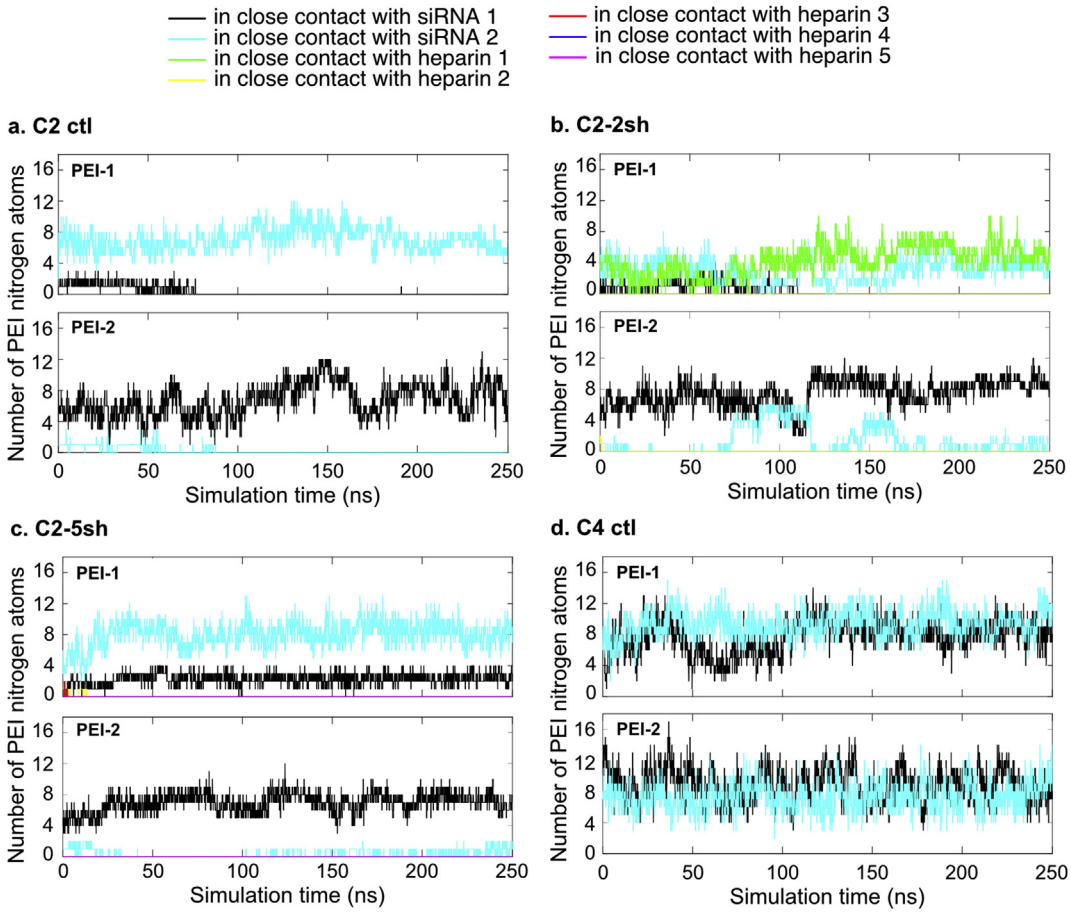

Fig. 6. Number of PEI N atoms within 4 Å of any siRNA and/or heparin N/O atoms as a function of simulation time in systems (**a**) C2 ctl, (**b**) C2-2sh, (**c**) C2-5sh, (**d**) C4 ctl. Two plots in each subfigure represent two separate PEIs (black and cyan curves corresponding to two separate siRNA molecules). The two and five heparin molecules in systems C2-2sh and C2-5sh, respectively, are presented with green, yellow, red, blue and purple curves. (For interpretation of the references to colour in this figure legend, the reader is referred to the web version of this article).

molecule charge density are the key differences [53]. To investigate PEI binding to these polyanions, we followed the same definition of bound PEI Ns as in Section 3.1, and used the percentage of bound Ns (out of the total PEI N atoms, Table S4; Supporting Information) to quantify PEI-siRNA and PEI-heparin binding in Fig. 7a. There was an inverse correlation between PEI's binding to siRNA and heparin; that is, if PEI binding to heparin is stronger, its binding to siRNA is weaker.

Among the systems with 568 Da PEI, maximal PEI binding to heparin is observed in C2-2lh with the average value of ~37%. Analysis of the PEI dynamics has shown that one of the 21-mer heparins is detaching one of the bridging PEIs at ~190 ns, and remains solely bound to this PEI afterwards (Fig. S7a; Supporting Information). This also explains the lowest PEI-siRNA binding observed in this system as one of the PEIs completely loses its contact with both siRNAs for about 60 ns (out of 250 ns simulation time in total). Decreasing the length of the heparin molecule from 21-mer to 12-mer (C2-2sh) decreased heparin's binding to PEI by 10%, and this resulted in a subsequent increase in PEI-siRNA binding. On the other hand, increasing the number of the short (12-mer) heparin molecules from low to moderate (C2-2sh vs. C2-5sh) completely hindered PEI-heparin binding, possibly due to MD related artifacts as discussed above. The lack of PEI-heparin binding was reflected in the strong PEI-siRNA binding; the comparison between systems C2-2sh and C2-5sh shows about 15% increase in PEI-siRNA binding in system C2-5sh.

Among the systems with 568 Da PEI, C1-7sh possesses the highest number of PEI molecules to achieve PEI/siRNA ratio >1. The abundance of PEI in the periphery of the complex results in a limited amount of space for each PEI to interact with the siRNAs. This gives rise to the surface PEIs being loosely bound to the siRNAs, as opposed to the PEIs amidst the two siRNAs establishing strong contacts with siRNAs (bridging PEIs). Close monitoring of the PEI dynamics in system C1-7sh (Fig. S6; Supporting Information) has revealed one of the surface PEIs (PEI-1) being detached from the complex by two heparins (heparin-5 and heparin-6) almost immediately after the simulation began (~10 ns). The interaction between heparin-6 and PEI-1 was maintained from the moment of their initial binding, whilst the binding between heparin-5 and PEI-1 was unstable. It appears that the length of the heparin is an important contributor to its binding strength to PEI, while 21-mer heparin was capable of detaching a strongly bound, bridging PEI (C2-2lh), under the same conditions, 12-mer heparin was unable to do so (C2-2sh). However, when 12-mer heparin interacted with loosely bound surface PEIs (C1-7sh), it was able to disengage the PEI from the complex surface. PEIs at different locations in the complex possess different binding strength to siRNA, which is another major factor impacting PEI binding affinity/strength toward heparin.

All the systems containing 1874 Da PEI displayed similar levels of PEI-siRNA and PEI-heparin binding. The ability of heparin to detach PEI was not evident on the 1874 Da PEI (Figs. S7b–d; Supporting Information). This suggests that MW of the PEI is

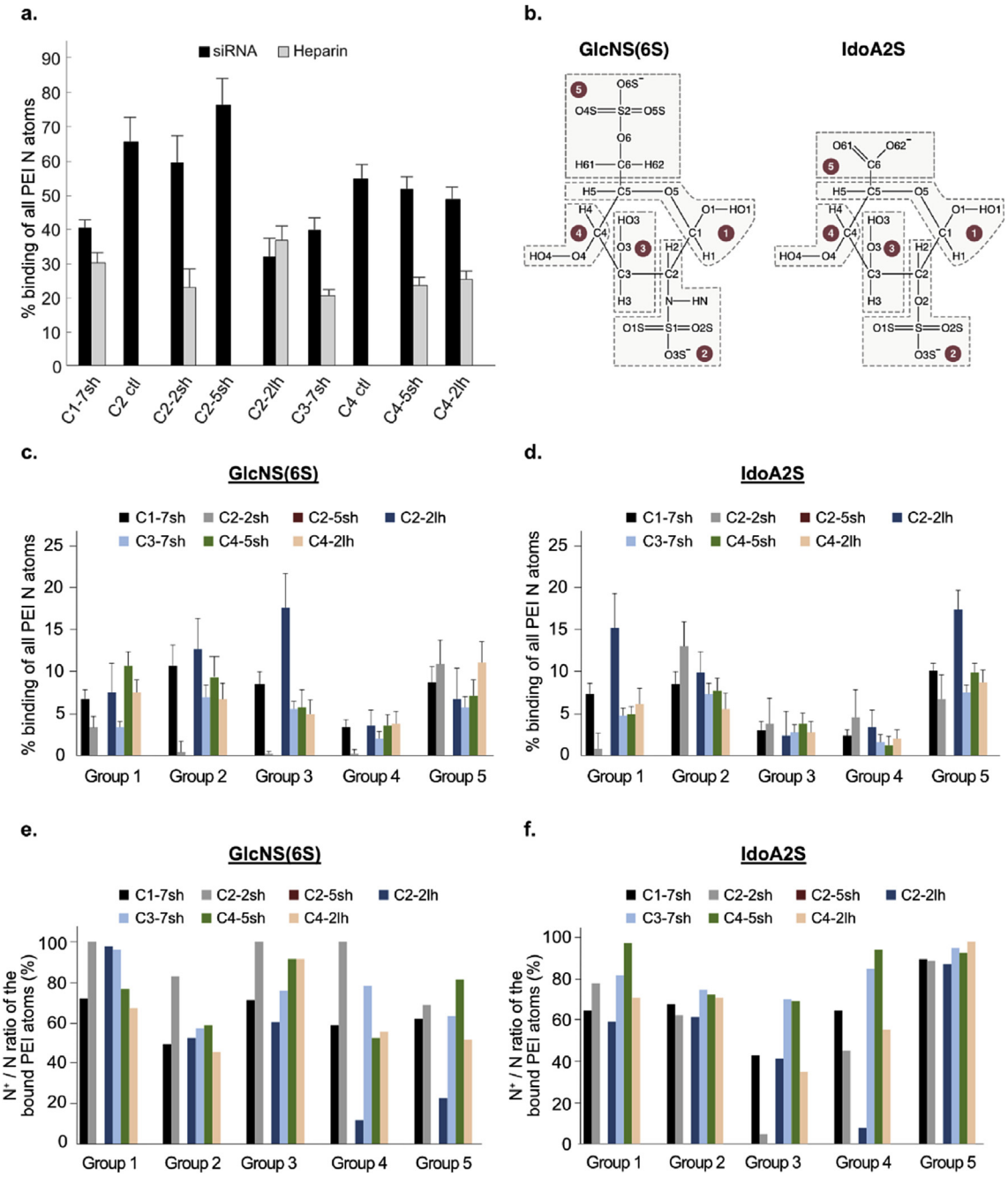

Fig. 7. (**a**) Percent binding of all PEI Ns to siRNA and heparin. Due to the higher number of PEI molecules in the systems with PEI/siRNA charge ratio ≥1 (thus higher number of PEI N atoms), the percentage of PEI binding to siRNA was found to be lower than that of the systems having PEI/siRNA charge ratio <1 (except for C2-2lh where PEI-siRNA binding is comparable), despite the presence of a higher number of Ns in bound state. (**b**) The individual groups in GlcNS(6S) and IdoA2S, where the summation of the atomic partial charges yields an integer group charge. Percent binding of all PEI N atoms to individual groups of heparin's building blocks (**c**) GlcNS(6S), and (**d**) IdoA2S. Percent contribution of the protonated PEI N atoms to overall PEI-heparin binding in (**e**) GlcNS(6S), and (**f**) IdoA2S. All the presented data in **(a)**, **(c)**, **(d)**, **(e)**, and **(f)** are average values over the final 50 ns of the simulations.

critical for the heparin's destabilizing effect on siRNA complexes.

Next, we examined the binding between the individual groups of heparin and PEI to assess the contribution of each group in binding. To do so, we first divided each heparin residue, GlcNS(6S) or IdoA2S, into five groups, where the summation of the atomic partial charges yields an integer group charge (Fig. 7b). Group 2 and Group 5 are the anionic groups, each carrying an overall charge of −1. Group 2 comprises a sulfamate moiety in GlcNS(6S), and a sulfate moiety in IdoA2S; whereas Group 5 contains a sulfate moiety in GlcNS(6S), and a carboxylate in IdoA2S. Group 3 has an overall neutral charge. Groups 1 and 4 are the connection points between the two residues in the heparin molecule, i.e., 1 → 4 linkage, their overall charge can differ depending on whether they undertake a linking role (−0.18 for Group 1 and 0.18 for Group 4) or remain as isolated residues at the two ends of the molecule (neutral). In Fig. 7c and d, we plotted the %binding of all the PEI Ns to designated groups in GlcNS(6S) and IdoA2S, respectively (see Table S4 for actual number of PEI Ns bound to each group). Based on

the analysis in Fig. 7c and d, Group 4 is the least contributing group to PEI binding, given that it is a small group residing in the 1 → 4 linkage. Group 1 exhibited considerable PEI binding levels in both GlcNS(6S) and IdoA2S residues, whereas Group 3 binding was more complex, its contribution was considerable in GlcNS(6S) but very little in IdoA2S. The anionic Group 2 and Group 5 were substantial contributors to PEI binding.

The strong binding demonstrated by the anionic groups brings up the question whether this behavior is a result of the electrostatic interactions between the anionic sulfate, sulfamate, or carboxylate moieties of heparin and the protonated Ns in PEI. In Fig. 7e and f, we plotted the percent contribution of the protonated PEI Ns to overall PEI-heparin binding (the actual number of PEI protonated Ns bound to the heparin groups is given in Table S4, along with the their % binding in Figs. S8a and b, in Supporting Information). Protonated Ns of PEI are expected to form electrostatic interactions with the anionic groups of heparin, as well as with the heparin atoms carrying negative partial charges. It could be seen from Fig. 7e and f that heparin's two building blocks, GlcNS(6S) and IdoA2S, display marked differences in their ability to establish electrostatic interactions with the protonated PEI Ns despite their equal anionic charge. Starting with the Group 2 of IdoA2S (a sulfate moiety), it was observed that 60–75% of the PEI-Group 2 binding comes from direct contacts with the protonated Ns of PEI (Fig. 7f). Having a sulfamate moiety in position 2 in GlcNS(6S), however, slightly hinders Group 2's ability to form electrostatic interactions, and reduces the electrostatic contribution to PEI-Group 2 binding to 45–60%, except for system C2-2sh (Fig. 7e). PEI-Group 5 binding displays even more marked differences between GlcNS(6S) and IdoA2S; the carboxylate moiety of IdoA2S is responsible of 87–98% of the overall PEI-Group 5 binding, as opposed to the GlcNS(6S)'s sulfate moiety where the corresponding contribution fluctuates from 23 to 81%, mostly localizing around 60%. The pattern observed in the electrostatic interactions was reflected in the H-bonds formed between the heparin's groups and the PEI Ns (Figs. S8c and d). Groups 2 and 5 displayed the highest number of H-bonds per PEI N, while the number of H-bonds formed by Groups 1 and 3 were significantly less, but comparable to each other. Group 4 was identified as the least contributor. The carboxylate of IdoA2S was again the most prominent group leading the H-bond interactions with PEI Ns.

The anionic moieties of heparin possess acid dissociation constants (pKa) in the range of 0.5 and 1.5 for the sulfate groups, and 2.0–4.0 for the carboxylates [54]. Given that the carboxylates are inherently weaker acids than the sulfates [55], one might expect sulfate containing groups dominating the binding of heparin to other biomolecules [1]. On the other hand, different moieties of heparin other than the sulfates could be essential for heparin binding [56]. We have observed that the carboxylate moiety of the iduronic acid is a major contributor to PEI binding. However, given the abundancy of sulfated groups in heparin (three sulfate moieties in the repeating disaccharide), the contribution to overall PEI binding from all the sulfated groups combined could be more than that of the carboxylate. The mechanism for the difference between the binding of sulfate and the carboxylate moieties remains to be explored. It is possible that the conformational flexibility of the internal iduronic acid pyranose rings [57,58] may lead to the positioning of the carboxylates that is favorable for PEI binding, or the steric hindrance brought by the bulky sulfates might be hindering their interactions.

3.3. Mechanistic insights into heparin mediated complex disassembly

Our simulation trajectories revealed that siRNA-PEI complexes display different responses to the presence of heparin in their periphery. We evaluated the response of each system by monitoring the motion of the siRNAs and the heparin's mode of action. The motion of the siRNAs was examined to see if the siRNAs remain complexed, or become partially relaxed or separated, whereas the heparin's action was determined from its binding to PEI, its PEI detachment activity, or its free floating motion in the bulk solution. These key observations are summarized in Table 2. There exists a clear distinction for the systems with different PEI MW; systems containing 568 Da PEI were found to be more vulnerable to the destabilizing effects of heparin, displaying a variety of different siRNA motions contingent on the heparin-related variables, whereas in 1874 Da PEI systems, the siRNAs remained in complex regardless of the heparin length or number of heparin molecules. Along the same lines, heparin's PEI detachment action can be seen in the 568 Da PEI systems, whilst PEI disengagement from the 1874 Da PEI bearing complexes was not possible. This puts great emphasis on the size of the carrier to resist heparin mediated destabilization. In support of this observation, Bertschinger and coworkers have previously shown that the amount of heparin bound to the branched PEIs correlated well with increase in PEI MW from 2 kDa, to 25 kDa and 750 kDa, thus a higher heparin concentration was needed to release the DNA bound to higher MW PEIs [59]. Kwok and Hart reported that DNA complexes containing 25 kDa branched PEI were more stable against heparin-mediated disassembly, requiring about 4 times higher heparin concentration than that for 22 kDa linear PEI to reach 95% dissociation [60]. Schaffer and coworkers investigated the dissociation of plasmid DNA complexes formed with polylysines possessing different lengths ranging from 19 to 180 residues. They demonstrated that complexes with shorter polymers can fully and more quickly be dissociated when exposed to excess amounts of immobilized double-stranded DNA, while only 50% dissociation was detected in the complexes formed with the longest (180 residue) polylysine [61]. Along the same lines, Danielsen and coworkers reported easier dissociation of DNA – low degree of polymerized chitosan complexes by heparin than the complexes from longer chitosan [62].

Among the 568 Da PEI systems, it could be seen that the change in the complex integrity is related to PEI/siRNA charge ratio and heparin length. Having the PEI/siRNA charge ratio >1 delivered a more stable complex, where shorter heparins were observed to disengage the loosely bound surface PEIs, but not the PEIs undertaking siRNA bridging role. The loss of a surface PEI did not induce any significant change in the complex stability, as there were still plenty of PEIs maintaining the overall integrity. Decreasing the number of PEIs (i.e. lowering the PEI/siRNA charge ratio below unity), however, induced instability within the complexes. At such low charge ratios, the complexes do not bear a net positive charge; moreover, due to the lack of PEIs, much of the complex is exposed to the surrounding solvent. Consequently, there exist repulsive forces between siRNAs and the peripheral heparin molecules. The absence of excess PEI also provides an easy access of heparin to the siRNA-bridging PEIs; the competing electrostatic attractions between the heparin and accessible PEIs negatively impact (or further sensitize) the stability of the complexes. The separation of the siRNAs was dependent on the amount of heparin as well as the length of the heparin chain. 12-mer heparin triggered the separation of the siRNAs when the number of heparin molecules in the system is low, whereas having excess heparin in the periphery did not allow for the full separation of the siRNAs, only permitting the partial relaxation. Owing to its longer chain length, hence higher negative charge, at the same amount of heparin molecules in the system, 21-mer heparin displayed stronger destabilizing action than its 12-mer counterpart by disengaging a bridging PEI from the

Table 2
Summary of the behavioral patterns observed in the studied systems. The orange icons represent the state of siRNAs, whereas the blue icons demonstrate heparin's mode of action.

Intact siRNAs
Partial relaxation of siRNAs
Separation of siRNAs
Heparin binding to PEI
Heparin detaching PEI
Free floating heparin in solution

	PEI/siRNA charge ratio	PEI M.W.	Heparin length	Heparin conc.	Observed phenomena
C1-7sh	1.05	568 Da	12-mer	High	
C2-2sh	0.15	568 Da	12-mer	Low	
C2-5sh	0.15	568 Da	12-mer	Moderate	
C2-2lh	0.15	568 Da	21-mer	Low	
C3-7sh	1.00	1874 Da	12-mer	High	
C4-5sh	0.50	1874 Da	12-mer	Moderate	
C4-2lh	0.50	1874 Da	21-mer	Low	

complex.

In the light of the different behavioral patterns demonstrated by our simulation systems, we propose the following five-stage mechanism for heparin-mediated disassembly of the siRNA-PEI complexes: (*i*) heparin binding to complex, (*ii*) detachment of surface PEIs, (*iii*) disengagement of bridging PEIs, (*iv*) change in siRNA torsional motion and partial relaxation of the complexes, and (*v*) separation of siRNAs (Fig. 8). We articulate that stages I and II are prerequisites for heparin-mediated relaxation/disassembly process to take place, via the loss of the protective PEI shell surrounding the siRNA cargo. It is important to note that the sequence of some of the proposed events does not necessarily have to be in this particular order; e.g. stages (*iv*) and (*v*) may happen simultaneously or one after the other; and some of the proposed stages may not be readily observed such as the detachment of the bridging PEIs.

3.4. Implications

Our methodology in varying the preparation variables has led to the sampling of different conformational states at the atomistic level. In Fig. 9, we schematically illustrate the free energy landscape of siRNA-PEI-heparin complexes in explicit water. From the analysis of many atomistic trajectories, we observed three main metastable conformational states; namely (*i*) heparin coated stable siRNA-PEI complex, (*ii*) stable siRNA-PEI complex with partially removed PEIs (surface bound and/or bridging), and (*iii*) relaxed or disassembled complex. As these states are derived from the simulation trajectories of different compositions, we are unable to decide which one of the metastable states is thermodynamically more stable than the others. Therefore, we present all the observed states as if they possess the same level of thermodynamic stability, however, in reality, some conformations might be more favorable than the others.

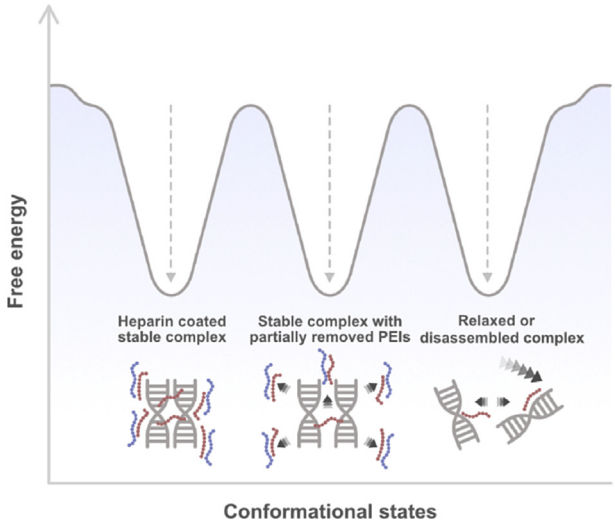

Fig. 9. Proposed conformational states of the siRNA-PEI-heparin ternary systems in explicit water. The representative siRNAs are given in gray, and representative PEIs and heparins are given in red and blue, respectively. (For interpretation of the references to colour in this figure legend, the reader is referred to the web version of this article).

The atomistic details of the ternary systems acquired from our MD simulations have shown that siRNA-PEI complexes experience a variety of heparin-mediated changes in their conformational states. Due to complex effects of GAGs on the complexes, previously conducted experimental studies have assigned contradictory roles to GAGs in the context of polynucleotide-based therapeutics. Our simulations have shown that heparins bind to siRNA-PEI complexes

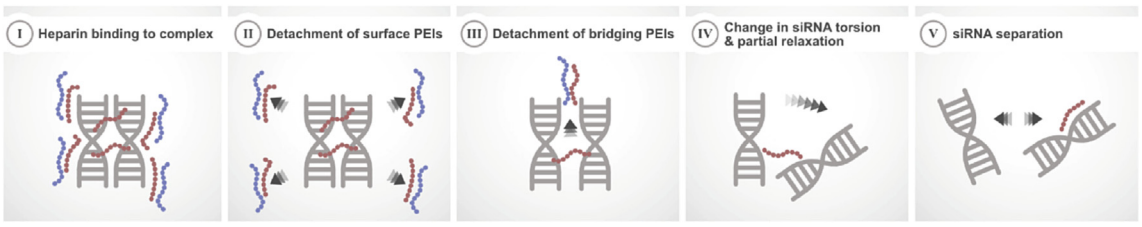

Fig. 8. The proposed mechanism for the heparin-mediated siRNA-PEI complex disassembly. The representative siRNAs are given in gray, and representative PEIs and heparins are given in red and blue, respectively. (For interpretation of the references to colour in this figure legend, the reader is referred to the web version of this article).

through electrostatic interactions and H-bonding with PEIs. The surface of the complexes becomes coated with heparin molecules in the presence of abundant peripheral PEIs, therefore the positive surface charge of the complex is sequestered by the heparins. This could be beneficial to reduce the cytotoxicity of the complexes, as the cationic charge of the PEI is mainly responsible for inducing damage to cell membranes and endocytic compartments [63]. If the complexes remain stable and coated with heparin (one of the proposed metastable states depicted in Fig. 9) prior to binding to the membrane milieu, heparins adsorbed on complex surfaces may explain the effects related to reduced cytotoxicities [8].

When heparin is present on cell surfaces in the form of heparin sulfate proteoglycans (HSPG), the attractive forces between highly anionic HS chains and the cationic complexes could facilitate cellular uptake of complexes [64]; GAGs may act as “receptors” in this case [5,6]. Along the same lines, previous dissipative particle dynamics simulations have shown that increasing the anionic lipid content of the cell membrane facilitates the uptake of the DNA containing cationic nanovectors through enhanced attraction to cell membrane, thereby decreasing the total engulfment time [65]. Hence, it is possible that the uptake of the complexes can take place more quickly and more efficiently in the presence of cell surface HSPGs. Since cells and tissues display a great variety in their GAG size and content [66], our simulations suggest that the number of heparins/HSPGs present on the cell surface and the length of heparin/HS GAG chains may critically influence the strength of the interactions and the resulting cellular uptake efficiency of complexes, as also suggested by Ruponen and coworkers [15]. On the other hand, cell surface GAGs may also disrupt the integrity of the complexes, by detaching the surface and bridging PEIs; the extent of this effect is dependent on GAG chain length, as well as the MW of the carrier and the cationic charge of the complex.

Binding of heparin to the polynucleotide complexes may also affect the subsequent intracellular trafficking events [14–16]. Shielding of the PEI cationic charges may adversely affect endosomal escape ability of PEI, and can eventually trap the complexes in the endocytic compartments. Complexes may experience heparin mediated partial relaxation and/or disassembly as shown by our MD simulations, which will make them more susceptible to the destabilizing effects of the pH changes in endosomes, hence they may be prematurely degraded. On the other hand, if the partially relaxed complexes could manage to escape from the endosomes, their disassembly in the cytosol, a key rate-limiting step to polynucleotide delivery, may have been facilitated by the relaxation that is already initiated by heparin.

3.5. Limitations

The size and time scale limitations brought by classical all-atom MD makes it highly challenging to study the dynamics of real-size supramolecular assemblies. With techniques such as coarse graining (CG) [67], it is possible to study systems of larger sizes by grouping a number of atoms together into “CG beads”, thus decreasing the degrees of freedom. Such an approach, however, causes the loss of atomistic representation of the system to some extent. As the aim of this study was to determine the nature of the atomistic interactions between the siRNA-PEI complexes and heparin, and to identify the conditions leading to conformational changes in the complexes, the simulations were performed at the all-atom level. The choice of the PEI and heparin was, thus, made accordingly to be of low MW. Although low MW PEIs are ineffective in delivering their nucleic acid cargo [68]; they possess low cytotoxicity profile and can be derivatized to match or exceed the performance of 25 kDa PEI after substitution with hydrophobic moieties, such as propionic acid [34]. Moreover, we expect the nature of interactions formed between PEI and heparin to remain the same, regardless of the PEI MW. It should be emphasized, however, heparin's PEI detachment action is dependent on the size of the PEI; as discussed, lower MW PEIs are more prone to heparin-mediated disengagement from their complexes with siRNA.

The PEI molecules simulated in this work carry a fixed charge of 46% amine protonation. The PEI/siRNA charge ratio is varied by changing the number of PEIs within the complex, at fixed number of siRNAs. Considering the increase in the simulation box size upon addition of heparin to the periphery of complexes, the maximum PEI/siRNA charge ratio is kept at ~1, corresponding to a PEI/siRNA weight ratio of ~0.3. From gel electrophoresis mobility shift assays, we previously reported complete binding of 2 kDa PEI to siRNA at the PEI/siRNA weight ratio of 0.4 [19]; hence, in the complexes bearing PEI/siRNA charge ratio ~1, the PEIs should display almost complete siRNA binding. Practically, the PEI/siRNA charge ratio is kept at an excess (see Ref. 69–72 that report N/P ratios ranging from 6 to 80) to ensure full protection of the siRNA cargo en route. However, it is not practical to simulate systems of such large sizes with all-atom MD simulations. Furthermore, we expect that the 5-step mechanism proposed for the heparin-mediated siRNA-PEI complex disassembly can still be applied to the systems bearing excess charge ratios, although more heparin molecules may be required to observe the entire process. It is worthwhile to note that as the number of surface PEIs increases, the process of disassembly may occur at a slower pace; given that the detachment of surface PEIs is necessary for the exposure of interior PEIs to heparin, which ultimately leads to the complete separation of the siRNAs via the loss of polyion bridging.

Among the systems bearing different PEIs and PEI/siRNA charge ratios, the destabilizing action of heparin was most prominent in the systems with low MW PEI and PEI/siRNA charge ratio below unity. Under experimental conditions, heparin was reported to dissociate the complexes in a concentration dependent manner; even at high polymer/nucleic acid charge ratios ($\gg 1$), the complexes can be dissociated at a sufficiently high heparin concentration [9]. However, within the size and time scale attainable with all-atom MD simulations, it is not practical to increase the heparin concentration, as this will give rise to technical problems such as the artificial periodicity mentioned in Section 3.1. In addition, the experimental time scale for heparin mediated changes on nucleic acid complexes lies between 15 min [12] to 2 h [62]; therefore, it is highly challenging to visit all possible transitional states under traditional MD settings (time less than one μs). Given the complexity of the supramolecular assemblies, the risk for the systems to be trapped in deep energy wells, unable to sample other possible conformational states, always exists. Enhanced sampling techniques such as replica exchange MD [73], accelerated MD [74], or metadynamics [75] to name a few, could be employed to overcome the high energy barriers between metastable states, as well as to increase the time scale of the simulations. We should note that, our efforts to sample more conformational states in the system C3-7sh by a simulated annealing [76] approach, i.e., gradually heating the system to 330 K, followed by full dynamics at 330 K for 50 ns, and then gradually cooling the system down to 300 K, did not result in any significant changes in the structure of the complexes (data not shown).

Despite the technical challenges, our methodology allowed us to observe some of the transitional states the complexes undergo both in the presence and absence of heparin. By varying the physical properties of the simulation systems and simulating as many trajectories of different compositions as possible, we were able to provide a full picture of the heparin-mediated disassembly of the siRNA-PEI complexes. In addition, we identified the critical parameters regulating the process of disassembly: PEI MW, PEI/siRNA

charge ratio, heparin length and concentration. Some of these parameters (PEI MW, PEI/siRNA charge ratio, heparin concentration) were previously identified through physicochemical studies, and on these aspects, our study provided a computational validation to the experimentally observed phenomena. Due to the challenges arising from the poor characterization of commercial heparin and lack of atomic resolution in most physicochemical assays, the molecular interactions between heparin and siRNA-PEI complexes were not fully known to date. By investigating these interactions at the all-atom level, we demonstrated the electrostatic origin of the heparin – siRNA-PEI complex interactions, and revealed, for the first time, the influence of heparin's different anionic groups on binding to PEI.

4. Conclusions

The effect of heparin on siRNA-PEI nanoparticles has been elucidated from a series of all-atom MD simulations. We developed an approach to study the transitional states of the siRNA-PEI-heparin ternary complexes to reveal a picture of the heparin-mediated changes in complex conformation. We found that heparin binds to siRNA-PEI complex through electrostatic interactions and H-bonding with PEI Ns. These interactions with PEI were mainly governed by the anionic $-N/O-SO_3^-$ and $-COO^-$ groups of heparin. The $-COO^-$ moiety of the iduronic acid residues was a major contributor to PEI binding. The MW of PEI and PEI/siRNA charge ratio in complexes were found to regulate the response to heparin. The chain length of heparin and the number of heparin molecules present in the system were critical. From these findings, we propose the following multi-step mechanism for heparin mediated disassembly of the siRNA-PEI nanoparticulate complexes: (*i*) heparin binding to complex, (*ii*) detachment of surface PEIs, (*iii*) disengagement of bridging PEIs, (*iv*) change in siRNA torsional motion and partial relaxation of the complexes, and (*v*) separation of siRNAs. We further propose three metastable states in the energy landscape of the ternary systems in explicit water, which are (*i*) heparin coated stable siRNA-PEI complex, (*ii*) stable siRNA-PEI complex with partially removed PEIs (surface and/or bridging), and (*iii*) relaxed or disassembled complex. These mechanistic observations should further facilitate design of new carriers for gene medicines and help to better understand the behavior of polynucleotide complexes in the physiological milieu.

Acknowledgements

Compute Canada and WestGrid are gratefully acknowledged for providing the computing resources and technical support. We thank Dr. Morteza Chelel Amirani for the determination of the restrained electrostatic potential charges of a heparin residue from quantum mechanical calculations. This work is funded by Natural Sciences and Engineering Research Council of Canada (NSERC) (RGPIN 04460, RGPIN 341907), NSERC Collaborative Research and Training Experience Program for Regenerative Medicine (NCPRM), Canadian Institutes of Health Research (CIHR) (MOP 74452), Alberta Innovates Technology Futures (AITF), and Canada Foundation for Innovation (CFI).

Appendix A. Supplementary data

Supplementary data related to this article can be found at https://doi.org/10.1016/j.biomaterials.2017.11.037.

References

[1] N.S. Gandhi, R.L. Mancera, The structure of glycosaminoglycans and their interactions with proteins, Chem Biol. Drug Des. 72 (2008) 455–482.
[2] L. Kjellen, U. Lindahl, Proteoglycans: structures and interactions, Annu. Rev. Biochem. 60 (1991) 443–475.
[3] J.T. Gallagher, M. Lyon, W.P. Steward, Structure and function of heparan sulphate proteoglycans, Biochem. J. 236 (1986) 313–325.
[4] R. Raman, V. Sasisekharan, R. Sasisekharan, Structural insights into biological roles of protein-glycosaminoglycan interactions, Chem. Biol. 12 (2005) 267–277.
[5] K.A. Mislick, J.D. Baldeschwieler, Evidence for the role of proteoglycans in cation-mediated gene transfer, Proc. Natl. Acad. Sci. U. S. A. 93 (1996) 12349–12354.
[6] L.C. Mounkes, W. Zhong, G. Cipres-Palacin, T.D. Heath, R.J. Debs, Proteoglycans mediate cationic liposome-DNA complex-based gene delivery in vitro and in vivo, J. Biol. Chem. 273 (1998) 26164–26170.
[7] D.E. Humphries, J.E. Silbert, Chlorate: a reversible inhibitor of proteoglycan sulfation, Biochem. Biophys. Res. Commun. 154 (1988) 365–371.
[8] M. Belting, P. Petersson, Protective role for proteoglycans against cationic lipid cytotoxicity allowing optimal transfection efficiency in vitro, Biochem. J. 342 (Pt 2) (1999) 281–286.
[9] M. Ruponen, S. Yla-Herttuala, A. Urtti, Interactions of polymeric and liposomal gene delivery systems with extracellular glycosaminoglycans: physicochemical and transfection studies, Biochim. Biophys. Acta 1415 (1999) 331–341.
[10] Y. Xu, F.C. Szoka Jr., Mechanism of DNA release from cationic liposome/DNA complexes used in cell transfection, Biochemistry 35 (1996) 5616–5623.
[11] C.M. Wiethoff, J.G. Smith, G.S. Koe, C.R. Middaugh, The potential role of proteoglycans in cationic lipid-mediated gene delivery. Studies of the interaction of cationic lipid-DNA complexes with model glycosaminoglycans, J. Biol. Chem. 276 (2001) 32806–32813.
[12] Y. Liu, T.M. Reineke, Poly(glycoamidoamine)s for gene delivery: stability of polyplexes and efficacy with cardiomyoblast cells, Bioconjug Chem. 17 (2006) 101–108.
[13] M. Belting, P. Petersson, Intracellular accumulation of secreted proteoglycans inhibits cationic lipid-mediated gene transfer. Co-transfer of glycosaminoglycans to the nucleus, J. Biol. Chem. 274 (1999) 19375–19382.
[14] M. Ruponen, S. Ronkko, P. Honkakoski, J. Pelkonen, M. Tammi, A. Urtti, Extracellular glycosaminoglycans modify cellular trafficking of lipoplexes and polyplexes, J. Biol. Chem. 276 (2001) 33875–33880.
[15] M. Ruponen, P. Honkakoski, M. Tammi, A. Urtti, Cell-surface glycosaminoglycans inhibit cation-mediated gene transfer, J. Gene Med. 6 (2004) 405–414.
[16] A. Nomani, Z. Hyvonen, E. Pulkkinen, M. Hiekkala, M. Ruponen, Intracellular gene delivery is dependent on the type of non-viral carrier and defined by the cell surface glycosaminoglycans, J. Control Release 187 (2014) 59–65.
[17] A. Barnard, P. Posocco, S. Pricl, M. Calderon, R. Haag, M.E. Hwang, V.W. Shum, D.W. Pack, D.K. Smith, Degradable self-assembling dendrons for gene delivery: experimental and theoretical insights into the barriers to cellular uptake, J. Am. Chem. Soc. 133 (2011) 20288–20300.
[18] M. Abbasi, A. Lavasanifar, L.G. Berthiaume, M. Weinfeld, H. Uludag, Cationic polymer-mediated small interfering RNA delivery for P-glycoprotein down-regulation in tumor cells, Cancer 116 (2010) 5544–5554.
[19] D. Meneksedag-Erol, T. Tang, H. Uludag, Probing the effect of miRNA on siRNA-PEI polyplexes, J. Phys. Chem. B 119 (2015) 5475–5486.
[20] J. Suh, H.J. Paik, B.K. Hwang, Ionization of poly(ethylenimine) and pol(allylamine) at various pH's, Bioorg Chem. 22 (1994) 318–327.
[21] S. Choosakoonkriang, B.A. Lobo, G.S. Koe, J.G. Koe, C.R. Middaugh, Biophysical characterization of PEI/DNA complexes, J. Pharm. Sci. 92 (2003) 1710–1722.
[22] J. Nagaya, M. Homma, A. Tanioka, A. Minakata, Relationship between protonation and ion condensation for branched poly(ethylenimine), Biophys. Chem. 60 (1996) 45–51.
[23] G.J.M. Koper, R.C. van Duijvenbode, D.D.P.W. Stam, U. Steuerle, M. Borkovec, Synthesis and protonation behavior of comblike poly(ethylenimine), Macromolecules 36 (2003) 2500–2507.
[24] J.D. Ziebarth, Y. Wang, Understanding the protonation behavior of linear polyethylenimine in solutions through Monte Carlo simulations, Biomacromolecules 11 (2010) 29–38.
[25] K. Utsuno, H. Uludag, Thermodynamics of polyethylenimine-DNA binding and DNA condensation, Biophys. J. 99 (2010) 201–207.
[26] L.E. Gerweck, K. Seetharaman, Cellular pH gradient in tumor versus normal tissue: potential exploitation for the treatment of cancer, Cancer Res. 56 (1996) 1194–1198.
[27] L.E. Gerweck, S. Vijayappa, S. Kozin, Tumor pH controls the in vivo efficacy of weak acid and base chemotherapeutics, Mol. Cancer Ther. 5 (2006) 1275–1279.
[28] Y. Kato, S. Ozawa, C. Miyamoto, Y. Maehata, A. Suzuki, T. Maeda, Y. Baba, Acidic extracellular microenvironment and cancer, Cancer Cell Int. 13 (2013) 89.
[29] J.L. Wike-Hooley, J. Haveman, H.S. Reinhold, The relevance of tumour pH to the treatment of malignant disease, Radiother. Oncol. 2 (1984) 343–366.
[30] C. Sun, T. Tang, H. Uludag, Molecular dynamics simulations of PEI mediated DNA aggregation, Biomacromolecules 12 (2011) 3698–3707.
[31] C. Sun, T. Tang, H. Uludag, Probing the effects of lipid substitution on polycation mediated DNA aggregation: a molecular dynamics simulations study, Biomacromolecules 13 (2012) 2982–2988.
[32] C. Sun, T. Tang, H. Uludag, Molecular dynamics simulations for complexation of DNA with 2 kDa PEI reveal profound effect of PEI architecture on complexation, J. Phys. Chem. B 116 (2012) 2405–2413.

[33] C. Sun, T. Tang, H. Uludag, A molecular dynamics simulation study on the effect of lipid substitution on polyethylenimine mediated siRNA complexation, Biomaterials 34 (2013) 2822–2833.
[34] D. Meneksedag-Erol, R.B. Kc, T. Tang, H. Uludag, A delicate balance when substituting a small hydrophobe onto low molecular weight polyethylenimine to improve its nucleic acid delivery efficiency, ACS Appl. Mater Interfaces 7 (2015) 24822–24832.
[35] J.C. Phillips, R. Braun, W. Wang, J. Gumbart, E. Tajkhorshid, E. Villa, C. Chipot, R.D. Skeel, L. Kale, K. Schulten, Scalable molecular dynamics with NAMD, J. Comput. Chem. 26 (2005) 1781–1802.
[36] B. Mulloy, M.J. Forster, C. Jones, D.B. Davies, N.M.R. and molecular-modelling studies of the solution conformation of heparin, Biochem. J. 293 (Pt 3) (1993) 849–858.
[37] Schrödinger Release 2015-4: Maestro, Schrödinger, LLC, New York, 2015.
[38] C. Sun, T. Tang, H. Uludag, J.E. Cuervo, Molecular dynamics simulations of DNA/PEI complexes: effect of PEI branching and protonation state, Biophys. J. 100 (2011) 2754–2763.
[39] K. Vanommeslaeghe, E. Hatcher, C. Acharya, S. Kundu, S. Zhong, J. Shim, E. Darian, O. Guvench, P. Lopes, I. Vorobyov, et al., CHARMM general force field: a force field for drug-like molecules compatible with the CHARMM all-atom additive biological force fields, J. Comput. Chem. 31 (2010) 671–690.
[40] O. Guvench, S.S. Mallajosyula, E.P. Raman, E. Hatcher, K. Vanommeslaeghe, T.J. Foster, F.W. Jamison 2nd, A.D. Mackerell Jr., CHARMM additive all-atom force field for carbohydrate derivatives and its utility in polysaccharide and carbohydrate-protein modeling, J. Chem. Theory Comput. 7 (2011) 3162–3180.
[41] W.B. Yu, X.B. He, K. Vanommeslaeghe, A.D. MacKerell, Extension of the CHARMM general force field to sulfonyl-containing compounds and its utility in biomolecular simulations, J. Comput. Chem. 33 (2012) 2451–2468.
[42] M.J. Frisch, G.W. Trucks, H.B. Schlegel, G.E. Scuseria, M.A. Robb, J.R. Cheeseman, G. Scalmani, V. Barone, B. Mennucci, G.A. Petersson, et al., Gaussian 09, Revision A.1, Gaussian Inc, Wallingford, CT, 2009.
[43] B.R. Brooks, R.E. Bruccoleri, B.D. Olafson, D.J. States, S. Swaminathan, M. Karplus, CHARMM - a program for macromolecular energy, minimization, and dynamics calculations, J. Comput. Chem. 4 (1983) 187–217.
[44] A.D. MacKerell, B. Brooks, C.L. Brooks, L. Nilsson, B. Roux, Y. Won, M. Karplus, CHARMM: the energy function and its parameterization with an overview of the program, in: Encyclopedia of Computational Chemistry, John Wiley & Sons, Chichester, UK, 1998, pp. 271–277.
[45] N. Foloppe, A.D. MacKerell, All-atom empirical force field for nucleic acids: I. Parameter optimization based on small molecule and condensed phase macromolecular target data, J. Comput. Chem. 21 (2000) 86–104.
[46] A.D. MacKerell, N.K. Banavali, All-atom empirical force field for nucleic acids: II. Application to molecular dynamics simulations of DNA and RNA in solution, J. Comput. Chem. 21 (2000) 105–120.
[47] T. Darden, D. York, L. Pedersen, Particle mesh Ewald - an N.Log(N) method for Ewald sums in large systems, J. Chem. Phys. 98 (1993) 10089–10092.
[48] J.P. Ryckaert, G. Ciccotti, H.J.C. Berendsen, Numerical integration of Cartesian equations of motion of a system with constraints: molecular dynamics of n-alkanes, J. Comput. Phys. 23 (1977) 327–341.
[49] W. Humphrey, A. Dalke, K. Schulten, VMD: visual molecular dynamics, J. Mol. Graph 14 (33–38) (1996) 27–38.
[50] E. Vuorimaa, A. Urtti, R. Seppanen, H. Lemmetyinen, M. Yliperttula, Time-resolved fluorescence spectroscopy reveals functional differences of cationic polymer-DNA complexes, J. Am. Chem. Soc. 130 (2008) 11695–11700.
[51] T. Schlick, Molecular Modeling and Simulation: An Interdisciplinary Guide, Springer, New York, USA, 2010.
[52] M.A. González, Force fields and molecular dynamics simulations, Collect. SFN 12 (2011) 169–200.
[53] S.A. Smith, S.H. Choi, J.N. Collins, R.J. Travers, B.C. Cooley, J.H. Morrissey, Inhibition of polyphosphate as a novel strategy for preventing thrombosis and inflammation, Blood 120 (2012) 5103–5110.
[54] H.M. Wang, D. Loganathan, R.J. Linhardt, Determination of the pKa of glucuronic acid and the carboxy groups of heparin by ^{13}C-nuclear-magnetic-resonance spectroscopy, Biochem. J. 278 (Pt 3) (1991) 689–695.
[55] J.W. Park, B. Chakrabarti, Optical characteristics of carboxyl group in relation to the circular dichroic properties and dissociation constants of glycosaminoglycans, Biochim. Biophys. Acta 544 (1978) 667–675.
[56] F. Chevalier, R. Lucas, J. Angulo, M. Martin-Lomas, P.M. Nieto, The heparin-Ca^{2+} interaction: the influence of the O-sulfation pattern on binding, Carbohydr. Res. 339 (2004) 975–983.
[57] D.R. Ferro, A. Provasoli, M. Ragazzi, B. Casu, G. Torri, V. Bossennec, B. Perly, P. Sinay, M. Petitou, J. Choay, Conformer populations of L-iduronic acid residues in glycosaminoglycan sequences, Carbohydr. Res. 195 (1990) 157–167.
[58] B. Mulloy, M.J. Forster, Conformation and dynamics of heparin and heparan sulfate, Glycobiology 10 (2000) 1147–1156.
[59] M. Bertschinger, G. Backliwal, A. Schertenleib, M. Jordan, D.L. Hacker, F.M. Wurm, Disassembly of polyethylenimine-DNA particles in vitro: implications for polyethylenimine-mediated DNA delivery, J. Control Release 116 (2006) 96–104.
[60] A. Kwok, S.L. Hart, Comparative structural and functional studies of nanoparticle formulations for DNA and siRNA delivery, Nanomedicine 7 (2011) 210–219.
[61] D.V. Schaffer, N.A. Fidelman, N. Dan, D.A. Lauffenburger, Vector unpacking as a potential barrier for receptor-mediated polyplex gene delivery, Biotechnol. Bioeng. 67 (2000) 598–606.
[62] S. Danielsen, S. Strand, C. de Lange Davies, B.T. Stokke, Glycosaminoglycan destabilization of DNA-chitosan polyplexes for gene delivery depends on chitosan chain length and GAG properties, Biochim. Biophys. Acta 1721 (2005) 44–54.
[63] A.E. Nel, L. Madler, D. Velegol, T. Xia, E.M. Hoek, P. Somasundaran, F. Klaessig, V. Castranova, M. Thompson, Understanding biophysicochemical interactions at the nano-bio interface, Nat. Mater 8 (2009) 543–557.
[64] I. Kopatz, J.S. Remy, J.P. Behr, A model for non-viral gene delivery: through syndecan adhesion molecules and powered by actin, J. Gene Med. 6 (2004) 769–776.
[65] H.M. Ding, Y.Q. Ma, Design maps for cellular uptake of gene nanovectors by computer simulation, Biomaterials 34 (2013) 8401–8407.
[66] J.D. Esko, K. Kimata, U. Lindahl, Proteoglycans and sulfated glycosaminoglycans, in: A. Varki, R.D. Cummings, J.D. Esko, H.H. Freeze, P. Stanley, C.R. Bertozzi, G.W. Hart, M.E. Etzler (Eds.), Essentials of Glycobiology, second ed., Cold Spring Harbor Laboratory Press, Cold Spring Harbor (NY), 2009.
[67] M. Levitt, A simplified representation of protein conformations for rapid simulation of protein folding, J. Mol. Biol. 104 (1976) 59–107.
[68] W.T. Godbey, K.K. Wu, A.G. Mikos, Size matters: molecular weight affects the efficiency of poly(ethylenimine) as a gene delivery vehicle, J. Biomed. Mater Res. 45 (1999) 268–275.
[69] L. Wightman, R. Kircheis, V. Rossler, S. Carotta, R. Ruzicka, M. Kursa, E. Wagner, Different behavior of branched and linear polyethylenimine for gene delivery in vitro and in vivo, J. Gene Med. 3 (2001) 362–372.
[70] M.E. Bonnet, P. Erbacher, A.L. Bolcato-Bellemin, Systemic delivery of DNA or siRNA mediated by linear polyethylenimine (L-PEI) does not induce an inflammatory response, Pharm. Res. 25 (2008) 2972–2982.
[71] H.M. Aliabadi, B. Landry, P. Mahdipoor, C.Y. Hsu, H. Uludag, Effective down-regulation of breast cancer resistance protein (BCRP) by siRNA delivery using lipid-substituted aliphatic polymers, Eur. J. Pharm. Biopharm. 81 (2012) 33–42.
[72] J. Valencia-Serna, H. Gul-Uludag, P. Mahdipoor, X. Jiang, H. Uludag, Investigating siRNA delivery to chronic myeloid leukemia K562 cells with lipophilic polymers for therapeutic BCR-ABL down-regulation, J. Control Release 172 (2013) 495–503.
[73] Y. Sugita, Y. Okamoto, Replica-exchange molecular dynamics method for protein folding, Chem. Phys. Lett. 314 (1999) 141–151.
[74] D. Hamelberg, J. Mongan, J.A. McCammon, Accelerated molecular dynamics: a promising and efficient simulation method for biomolecules, J. Chem. Phys. 120 (2004) 11919–11929.
[75] A. Laio, M. Parrinello, Escaping free-energy minima, Proc. Natl. Acad. Sci. U. S. A. 99 (2002) 12562–12566.
[76] C. Tsallis, D.A. Stariolo, Generalized simulated annealing, Phys. A Stat. Theor. Phys. 233 (1996) 395–406.